energies

MDPI

Article

Thermo-Economic Analysis of a Hybrid Ejector Refrigerating System Based on a Low Grade Heat Source

Gianluca Lillo [1], Rita Mastrullo [1], Alfonso William Mauro [1,*], Raniero Trinchieri [2] and Luca Viscito [1]

[1] Department of Industrial Engineering, Federico II University of Naples—P. le Tecchio, 80-80125 Naples, Italy; gianluca.lillo@unina.it (G.L.); rita.mastrullo@unina.it (R.M.); luca.viscito@unina.it (L.V.)

[2] Ente per le Nuove tecnologie, Energia ed Ambiente (ENEA), Italian National Agency for New Technologies, Energy and Sustainable Economic Development, C.R. Casaccia—Via Anguillarese 301, 00123 Rome, Italy; raniero.trinchieri@enea.it

* Correspondence: alfonsowilliam.mauro@unina.it; Tel.: +39-081-7682198

Received: 12 December 2019; Accepted: 21 January 2020; Published: 23 January 2020

Abstract: The rising of the global energy demand requires the use of alternative energy conversion systems employing renewable sources. In the refrigeration and air conditioning fields, heat driven ejector systems represent a promising way to produce the cooling effect by using available low-grade temperature sources. In this paper, a thermo-economic analysis of a waste heat recovery hybrid ejector cycle (WHRHEC) was carried out. A thermodynamic model was firstly developed to simulate a WHRHEC able to obtain chilled water with a cooling load of 20 kW, by varying the working fluids and the pinch point values in the heat exchangers. Specific single- and two-phase heat transfer correlations were used to estimate the heat transfer surface and therefore the investment costs. The operative ranges that provide a reasonable compromise between the set-up costs and the cycle performances were then defined and compared to the current waste heat-driven technologies, such as absorption chillers and organic Rankine cycles (ORCs) coupled with vapor compression cycles (VCCs). The last part of the paper presents an economic analysis providing the map of the design (plant size) and contingent (specific cost of energy, waste heat availability) variables that lead to the economic convenience of a WHRHEC system when integrated to a conventional VCC plant.

Keywords: thermo-economic analysis; ejector; waste heat recovery

1. Introduction

In recent decades, there has been a growing interest by the international community for the reduction of the energy consumption and the environmental impact using renewable sources. In this regard, the increase of the global energy consumption in 2018 is nearly twice the average rate of growth since 2010, due to the development of the global economy and also higher heating and cooling demands in some parts of the world. Worldwide, the air-cooling in building applications showed a steep increase: in 2018 its energy demand tripled with respect to the 1990 values [1]. In the European Union (UE)zone, heating and cooling in buildings and industry accounts for half of the energy consumption [2]. For household applications, heating and hot water alone account for 79% of total final energy use (192.5 Mtoe). Although the air-cooling is a fairly small share of total final energy use, the demand from households and businesses such as the food industry continuously rises during the summer months, by showing a similar trend with time to air pollution and global warming. In the industry field, 70.6% of energy consumption (193.6 Mtoe) is currently used [2] for space and industrial process heating, 26.7% (73.3 Mtoe) for lighting and electrical processes such as machine

motors, and 2.7% (7.2 Mtoe) for cooling purposes. Regarding the energy sources, according to 2018 data from Eurostat [2], 75% of heating and cooling is still generated from fossil fuels while only 19% comes from renewable energy. In order to reduce the energy consumption, great efforts should be done to increase the electricity production from renewable sources or increasing the efficiency of the heat driven system using solar energy and waste heat.

1.1. State of the Art of Heat Driven System Technologies

1.1.1. Absorption Systems

Absorption systems can be used to produce the cooling effect and take advantage of waste heat from industrial large-scale process. Within this technology, single effect chillers using LiBr-Water as a working pair represent a solid and commercially developed solution. Henning [3] gives an overview of solar assisted air conditioning systems for the buildings, highlighting that the 59% of the cooling systems in Europe using solar collectors for air conditioning are absorption systems. Market available absorption cooling technologies can span from 50 to 200 kW with COP (coefficient of performance) in the range 0.3–1.2, as reported by Baniyounes et al. [4]. When single effect systems are considered, the coefficient of performance is ranging between 0.3 and 0.8 with heat source temperature varying between 80 and 120 °C. Higher COP values (up to 1.3) can be obtained using double effect systems and higher heat source temperatures (up to 180 °C). Güido et al. [5] show the performance on field of 27 absorption systems equipped with a control algorithm able to optimize the system performance. In most of the investigated conditions, they obtained COP values ranging between 0.7 and 0.8. Typical COP values in this case might reach 0.6–0.8 (up to 0.9–1.3 in the case of double effect systems) after a careful optimization of the system for large sized plants for the air-conditioning sector [6]. For industrial field, absorption systems using Water/Ammonia as a working pair can be considered, although in this case lower COP are expected (0.25–0.5) [6]. However, these cooling systems have some drawbacks: LiBr-Water absorption chillers give low performances when the generation temperature is lower than 90 °C. Moreover, serious corrosion problems occur at generation temperatures higher than 200 °C, as reported Hassan and Mohamad [7]. In addition, single-effect and double-effect H_2O–LiBr cooling cycles cannot operate at heat condensation temperatures of 50 °C due to the crystallization limit at low water concentrations [8]. Furthermore, the cooling temperature should reach 5 °C at high condensing temperatures due to the risk of crystallization of the working fluid [9]. The investment costs may vary greatly depending on specifications project and requirements like available space, building height, network length, and other constraints: for single effect absorption systems operating with LiBr-Water, the specific investments costs can vary within a range of 0.2–1.2 k€ for unit of cooling load for a plant size higher than 100 kW. Almost the same values characterize Water/Ammonia absorption systems with specific investment costs that can vary from 0.4 to 1.25 k€ kW^{-1}.

1.1.2. ORC Coupled to Vapor Compression Cycle (VCC) Systems

Heat driven feasible alternatives to the absorption chillers are thermo-mechanical cooling systems in which the waste heat is converted into mechanical work by an organic Rankine cycle (ORC) coupled with a vapor compression cycle (VCC). These systems have received a growing interest due to their advantages, since they carry beneficial effects by converting waste heat or heat from renewable sources into electricity enabling a better use of primary energy for cold production [10]. Furthermore, these systems have the capability to provide the cooling load also at low temperatures and to produce electricity when cooling is not needed [10]. In addition, these systems are suitable in a wide range of high temperature sources with an overall efficiency that can reach 0.6 [11]. The performance, however, decreases significantly with lower required loads [12]. From the recent scientific literature, the information about each single subsystem performance (ORC and VCC separately) are collected in order to obtain a combined ORC/VCC map in terms of investment costs (in a range 0.63–3.43 k€ kW^{-1}) [12] and overall performance (from 12.5% to 37.5%) [6].

1.1.3. Hybrid Ejector Systems

In the case of small-scale applications, waste heat recovery hybrid ejector cycles (WHRHEC) can represent an attractive solution especially for domestic end-users in which the solar energy could be realistically employed to produce the cooling effect. Most of the earlier studies in scientific literature concerning ejector refrigeration systems were carried out with working fluids having high global warming potential (GWP) values or ozone depletion potential (ODP) index greater than zero, such as R141b, R123, R245fa, and R134a. The first two are already banned according to the Montreal Protocol [13], while the remaining two will be phased out soon (European F-Gas regulation) [14]. R600 (butane), R600a (isobutane), and R290 (propane) have also been considered in theoretical studies as potential environmentally friendly refrigerants, even if these hydrocarbons have the drawback of a high flammability. As shown in theoretical work of Tashtoush et al. [15], the maximum generator temperature that can be used when employing R290 is about 95 °C, because of its low critical temperature of 96.7 °C. Additionally, R290 needs high pressures and robust construction when compared to other refrigerants. Hernandez et al. [16] theoretically studied the behavior of ejector cooling systems using blends R410A and R507, obtaining a higher COP (0.53) when refrigerant R410A is employed. There are both increased research and industrial development efforts to create environmentally friendly working fluids: in this regard, hydroflouro-olefin (HFO) refrigerants represent a new generation of refrigerants with a very low GWP and no ODP.

Chen et al. [17] presented a recent widespread state-of-the-art study on ejector technology while Besagni et al. [18] presented a review on ejector in refrigeration systems focusing on the ejector working principles and on the working fluids selection. The first experimental study of the ejector refrigeration system operating with isobutane (R600a) driven by low grade heat source was presented by Butrymowicz et al. [19]: their experimental results confirm that it is possible to use a WHRHEC driven by the heat distribution network. However, due to the low vapor generator temperature, a thermodynamic COP of 0.15 was obtained. In the work of Besagni et al. [20], the influence of the working fluids on the performance of a WHRHEC was theoretically studied by using a lumped parameter model. Their results show that different working fluids should be considered depending on the generator temperature: refrigerant R134a is suitable for low temperatures (<100 °C), hydrocarbons for medium temperatures (100–130 °C), and R601 (pentane) for high temperatures (>130 °C).

Zegenhagen and Ziegler [21] carried out an experimental investigation of an ejector refrigeration system operating with R134a, obtaining a system COP of 0.3. Wang et al. [22] studied a hybrid ejector-based refrigeration system using a low step compressor operating with R134a. They concluded that automobile air-conditioning represents a potential application since waste heat from internal combustion engines can be utilized as system thermal input. Various fluids such as R134a, R152a, R290, and R600a were investigated by Dahmani et al. [23]. Gil and Kasperski [24] studied the performance of an ejector system working with R236ea, R236ca, R245ca, R245fa, R356mfc, RC318, Acetone, Benzene, Cyclohexane, Cyclopentane, and Toluene concluding that, among the non-flammable synthetic refrigerants tested, R236fa showed the highest COP of 0.23 for a vapor generator temperature of 95 °C. Chen et al. [25] theoretically studied the performance of a WHRHEC considering R134a, R152a, R290, R430A, R245fa, R600, R600a, and R1234ze as working fluids, concluding that R245fa and R600 have the highest COP of 0.38. Tashtoush et al. [15] used a 1-D modeling approach based on the ideal gas model and examined the performance of an ejector system in superheated conditions with R152a, R290, R141b, R123, R600a, R600, R717, and R134a: the thermodynamic COP is in the range of 0.57–0.8 at 100 °C generator temperature, 24–27 bar generator pressure and 8–12 °C evaporator temperature. Roman and Hernandez [16] investigated an ejector system using R290, R152a, R134a, R600a, R600, and R123 as working fluids obtaining the highest COP when R290 was considered.

Recently, Śmierciew et al. [26] investigated the performance of R1234ze(E) in an ejector refrigeration system with thermal capacity of 90 kW able to provide 30 kW of cooling load driven by low grade heat source. Atmaca et al. [27] compared the performance of an ejector refrigeration system using R1234yf,

R1234ze(E), and R134a. The maximum COP was similar in the case of R1234ze(E) and R134a, but lower COP values were found using R1234yf.

However, due to their relative recent introduction in the market [28,29], studies on ejector refrigeration systems using HFO refrigerants are still limited in scientific literature. Furthermore, according to the current state of the art, there are no available economic data for the WHRHEC technology, and a cost/performance comparison with conventional heat driven systems already established in the market is therefore not presently feasible.

1.2. Aim of the Paper

The aim of the paper is two-fold:

1. To estimate performances and costs for the typical operating conditions of a waste heat recovery hybrid ejector cycle (WHRHEC). The results of the proposed thermo-economic analysis should be useful to place the WHRHEC systems among the actual heat driven cooling technologies available on the market, in terms of two conflicting goals (performance/investment costs).
2. To use the estimation of the performances and costs to evaluate the economical convenience of a waste heat recovery hybrid ejector cycle (WHRHEC) integrated to a conventional vapor compression cycle (VCC). The following economic analysis will give to the reader realistic information about the economic convenience in the use of the WHRHEC systems instead of traditional vapor compression cycles, when a certain amount of waste heat is available.

2. Hybrid Ejector Cycle: Modeling and Thermodynamic Analysis

In this paper, hot water from a renewable source (solar heating system) was used as the low-grade waste heat source to simulate the ejector cooling system. A schematic representation of the layout is shown in Figure 1a. The working fluid in saturated liquid condition is driven by an electric pump that pushes the refrigerant (point 1) in a counterflow internal heat exchanger, that uses the outlet ejector flow (point 5) to preheat the subcooled liquid before entering the vapor generator (point 1R), in which a temperature of 110 °C is reached (point 2). The high-pressure vapor from the generator, called primary flow, expands into the motive nozzle. The pressure at the motive nozzle outlet, being lower than the evaporator pressure, allows the entrainment of the low-pressure vapor from the evaporator, called secondary flow. The mixed flow at the outlet of the ejector is firstly cooled into the internal heat exchanger and then flows into the condenser. The saturated liquid at the outlet of the condenser is divided into two parts. The first part goes through the expansion device (reaching point 3) and then it evaporates (point 4) producing the cooling effect. The remaining part is pumped to the generator pressure. All the transformations occurring inside the ejector are described in detail in the following section. An example of the corresponding thermodynamic cycle on the T-s diagram is reported in Figure 1b. The thermo-physical properties are evaluating by using Refprop 9.0 software developed by NIST [30].

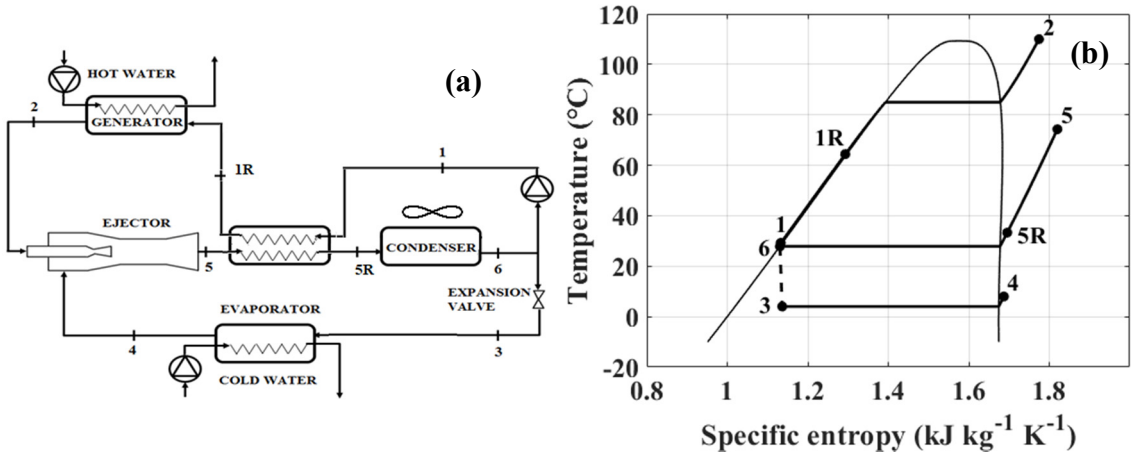

Figure 1. (**a**) Schematic layout. (**b**) Example of an ejector cooling cycle on T-s diagram for the fluid R1234ze.

The enthalpy of the mixed flow at the ejector outlet (point 5 in Figure 1b) is calculated by an energy balance on the ejector, once the ejector entrainment ratio is known by solving the ejector model, which is described in detail in the following paragraph.

$$h_5 = \frac{h_2 + \mu h_4}{1 + \mu} \tag{1}$$

The system performance is evaluated with the coefficient of performance (COP) expressed as follows with referring to the numeration in Figure 1. The electrical power required by the pump was neglected for the thermodynamic analysis.

$$COP = \frac{\dot{Q}_{ev}}{\dot{Q}_g} = \mu \frac{h_4 - h_3}{h_2 - h_{1R}}, \tag{2}$$

where $\dot{Q}_{ev}$ and $\dot{Q}_g$ are the heat power (kW) at the evaporator and at the generator, respectively, μ is the entrainment ratio (defined in the following section), and h is the refrigerant specific enthalpy (kJ kg^{-1}).

2.1. Ejector Model

To simulate the ejector performance, a one-dimensional method presented in the theoretical work of Chen et al. [31] is employed in the current optimization process. In this model, the mixing process of the flows occurs at constant pressure, lower than the evaporation level, by taking into account shock process inside the ejector. Ideal gas behavior is assumed to simplify the analytical description. The velocities of the primary and secondary flows are negligible before entering the ejector; also, the velocity of the mixed flow leaving the ejector is also neglected. Considering the numbering of Figure 2a, once the conditions at the intel of the primary (point 2) and secondary (point 4) flows and the ejector outlet pressure (point 5) are given, the model calculates the optimum entrainment ratio μ and the corresponding area ratio A_r.

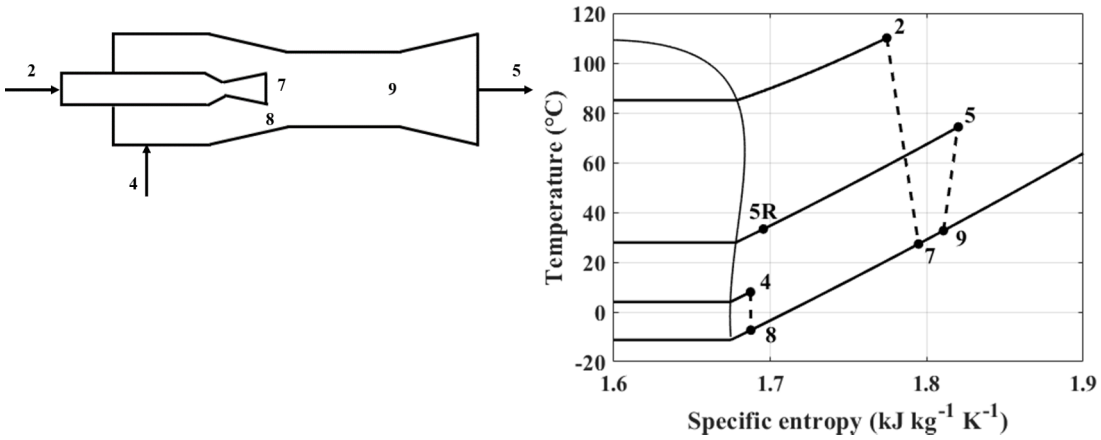

(**a**) (**b**)

Figure 2. (**a**) Schematic ejector representation. (**b**) Ejector working processes on the T-s diagram.

The entrainment ratio is an ejector performance indicator, which is defined in Equation (3) as the ratio of the secondary mass flow rate $\dot{m}_{sf}$ (kg s^{-1}) to the primary mass flow rate $\dot{m}_{pf}$ (kg s^{-1}). The expression of the entrainment ratio can be obtained from the conservation of the momentum [31], shown in Equation (3), once the losses inside the ejector in terms of isentropic efficiencies in the nozzle (η_N), in the mixing chamber (η_M), and in the diffuser (η_D) are defined.

The enthalpy of the point 7 h_7 represents the thermodynamic condition of the flow at the exit of the nozzle. It is evaluated by using the definition of the nozzle efficiency and the energy conservation between inlet and outlet of the nozzle [31]. The enthalpy of the point 8 h_8 (expansion of the secondary flow) is evaluated by applying the energy balance between the point 4 and 8 and considering an ideal process [31]. The velocity and the enthalpy of the mixed flow u_9 and h_9 are evaluated by combining energy and momentum balance between points 7, 8, and 9 [31]. The complete set of equations is available in the original reference [31].

According to the chosen method, constant values for ejector efficiencies are considered ($\eta_N = 0.9$, $\eta_M = 0.8$, $\eta_D = 0.9$) and defined in the following equations. The transformation occurring inside the ejector are shown on the T-s diagram in Figure 2b. The line 2–7 represents the expansion of the flow inside the motive nozzle taking into account the nozzle efficiency. Similarly, points 8 and 9 represent the end point of the real process inside the mixing chamber and the diffuser, respectively. The pressure in 7, 8, and 9 is the mixing pressure, which is lower than the secondary flow pressure.

$$\mu = \frac{\dot{m}_{sf}}{\dot{m}_{pf}} = \frac{\sqrt{2\eta_N(h_2 - h_{7s})} - \sqrt{\frac{2(h_{5s}-h_9)}{(\eta_D\eta_M)}}}{\sqrt{\frac{2(h_{5s}-h_9)}{(\eta_D\eta_M)}} - \sqrt{2(h_4 - h_8)}}\eta_N = \frac{h_2 - h_7}{h_2 - h_{7s}};\ \eta_M = \frac{u_9^2}{u_{9s}^2};\ \eta_D = \frac{h_{5s} - h_9}{h_5 - h_9}. \quad (3)$$

The area ratio A_r is defined as the ratio of the constant area section of the mixing chamber (A_m) to the nozzle throat area (A_t), and it is expressed by the following equation [31].

$$A_r = \frac{A_m}{A_t} = \frac{P_2(1+\mu)^{0.5}\left(1+\mu\frac{T_4}{T_2}\right)^{0.5}\left(\frac{2}{(k+1)}\right)^{\frac{1}{(k-1)}}\left(1-\frac{2}{(k+1)}\right)^{0.5}}{P_c\left(\frac{P_9}{P_5}\right)^{1/k}\left(1-\left(\frac{P_9}{P_5}\right)^{(k-1)/k}\right)^{0.5}}. \quad (4)$$

The mass flow rate of the primary flow through the nozzle is determined by Equation (5) [32] considering chocked conditions at the nozzle throat, where R represents the specific gas constant, A_t is the nozzle throat cross section, k is the heat capacity ratio, and η_N is the nozzle efficiency defined

previously. Once the primary flow rate is known, the nozzle throat section can be evaluated by using Equation (5).

$$\dot{m}_{pf} = P_2 \frac{A_t}{\sqrt{T_2}} \sqrt{\frac{k}{R}\left(\frac{2}{k+1}\right)^{\frac{(k+1)}{(k-1)}}} \sqrt{\eta_N}. \quad (5)$$

The pressure lift Π is defined as the ratio between the pressure at the outlet of the ejector and the pressure of the secondary flow rate, whereas β is the ratio between the pressure of the primary flow and the pressure at the ejector outlet.

$$\Pi = \frac{P_5}{P_4} = \frac{P_{co}}{P_{ev}}; \beta = \frac{P_2}{P_5} = \frac{P_{gv}}{P_{co}}.$$

2.2. Working Fluids

The properties of the working fluid influence the performance of the vapor compression cooling systems. An appropriate refrigerant can not only provide good system performance and therefore energy saving, but also involves less environmental issues. Basic considerations require eco-friendly working fluids (low OPD and GWP), safety issues, low cost, and availability. Furthermore, as reported in the work of Varga et al. [33], more specific prescriptions should be taken into account when choosing a working fluid for ejector cooling systems:

- high latent heat value in the evaporator and generator temperature range to minimize the mass flow rate per unit of heat power;
- relatively high critical temperature to make the system feasible in a wide range of generator temperatures;
- not too high saturation pressure in the generator and not too low in the evaporator.

Additionally, the slope of saturated vapor line should be considered. The use of dry refrigerant is recommended in order to avoid the development of droplets inside the ejector, which may block the effective area. In this analysis water was excluded, because of its rather low COP according to [33]. HFCs were also excluded due to their high GWP. Hydrocarbons as butane (R600) and isobutane (R600a), ammonia and new HFO refrigerants R1234ze and R1233zd were considered. The main thermophysical and environmental properties of the selected working fluids are listed in Table 1, according to Refprop 9.0 [30]. The corresponding saturation curves are reported in Figure 3.

Table 1. Characteristics of the selected working fluids.

Fluids	T_{cr} (°C)	P_{cr} (bar)	ASHRAE Classification	GWP	ODP
R1234ze	109.4	36.4	A2L	6	0
Ammonia	132.3	113.0	B2L	0	0
R1233zd	165.6	37.7	A1	1	0
Isobutane	134.7	36.4	A3	3	0
R134a	101.1	40.7	A1	1430	0
Butane	152.0	38.0	A3	4	0

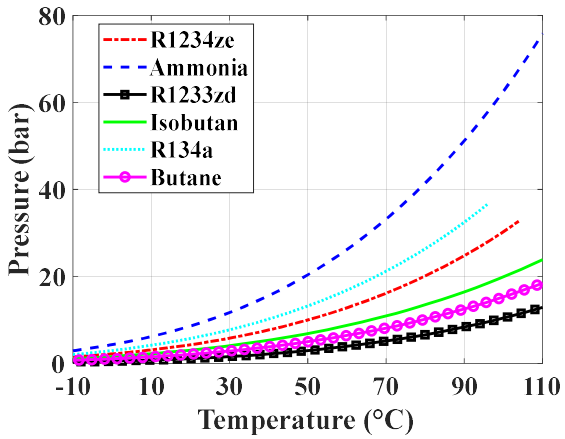

Figure 3. Saturation curves in the pressure-temperature diagram for the selected working fluids.

2.3. Thermodynamic Analysis: Conditions and Results

Using the ejector and the system model previously shown, 42 simulations were carried out in order to define an entrainment ratio map in terms of pressure lift and β ratio that provides the influence of several temperature differences at pinch point on the ejector performance for each investigated working fluid.

In particular, the hot water at the vapor generator inlet is supplied by considering a solar heating system able to produce hot water at 120 °C, as reported in the current literature [34,35]. For a given heat load, a too low temperature variation of the secondary flow at the vapor generator would require higher mass flow rates for the secondary fluid (and thus higher pumping costs) and also a lower refrigerant superheat, which could be too small to be plausibly controlled. On the contrary, a too high temperature variation would lead to low refrigerant saturation temperatures, strongly penalizing the thermodynamic cycle efficiency. Due to this fact, in this analysis an outlet temperature of the secondary fluid of 80 °C was chosen in order to take into account these two competing aspects.

The data used are listed in Table 2 and the simulated pinch points values are listed in the legend in the following figures. The low-pressure evaporating temperature is directly obtained from the chilled water temperature and the given pinch point value, whereas the evaluation of the remaining saturated conditions (condenser and high-pressure evaporator) are obtained with an iterative process seeking the exact pinch point provided. In a first step, the high temperature evaporation and condensation pressures were fixed at guessed values and the thermodynamic cycle was constructed. Then, the pinch point (occurring at saturated vapor and liquid for the condenser and the generator, respectively) was calculated and the pressures were accordingly changed, adjusting the guess values in order to obtain the design temperature difference. For instance, if the pinch point value is lower than the arranged one, the condenser/evaporator pressure has to be accordingly increased/decreased. All the thermodynamic and transport properties of refrigerants were evaluated through the software Refprop 9.0, developed by NIST [30].

Table 2. Specification of the simulated boundary conditions.

Simulated Conditions	Values
Cooling load (kW)	20
Water temperature at the vapor generator (inlet/outlet) (°C)	120/80
Air temperature at the condenser (inlet/outlet) (°C)	20/25
Water temperature at the evaporator (inlet/outlet) (°C)	12/7
Quality at condenser outlet	0.0
Working fluid temperature at vapor generator outlet (°C)	110
ΔT superheating at evaporator outlet (K)	4
Regenerative heat exchanger efficiency	0.90
Pump efficiency	0.70

Figure 4 shows the entrainment ratio μ map as function of the β ratio and pressure lift Π. The main objective of the following figures is to present the general trends as a function of the operating conditions indicated in the corresponding legends. Considering the working fluid R134a, the configuration with 1 K of pinch point for all heat exchangers was excluded since the temperature exceeded the critical value of 101.1 °C. The refrigerant R1233zd is characterized by higher values of Π and β due to lower saturation pressure at fixed temperature with respect to the other investigated fluids.

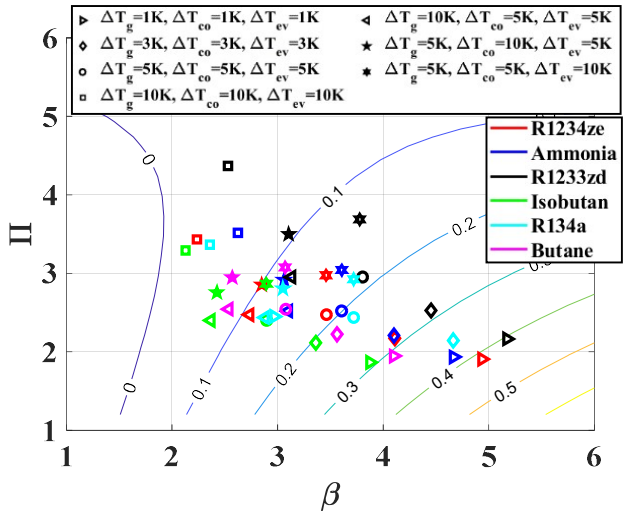

Figure 4. Entrainment ratio (contour plot) as a function of beta ratio and pressure lift for different pinch point values at the heat exchangers.

When the lower value of the temperature difference at the pinch point is considered for all heat exchangers, the maximum entrainment ratio is obtained for all refrigerants, reaching a value of 0.438 for R1233zd. The results shown in Figure 4 can be useful to identify the influence of the variation of each temperature difference at the pinch point by keeping constant the other two. Assuming as reference the configuration with all temperature differences at pinch point of 5 K for R1233zd, by increasing the pinch point from 5 to 10 K, lower values of the entrainment ratio are obtained. In particular, the highest reduction is obtained when the variation of the pinch point occurs at the condenser with the entrainment ratio passing from 0.210 to 0.097. In this case, the increase of the pinch point at the condenser negatively affects the β ratio, while increases the pressure lift: both the effects contribute to a drop of the entrainment ratio. Instead, when the pinch point at the vapor generator (or the evaporator) increases from 5 to 10 K, the entrainment ratio μ decreases from 0.210 to 0.151 (to 0.13 for the low-pressure evaporator).

Figure 5 shows the system COP as function of β and Π with a very similar trend with respect to the previous diagram. The system COP is in fact strictly related to the entrainment ratio due to its

definition as reported in Equation (2) and, with enthalpy variation ratio at the low and high pressure evaporators from 0.8 to 1.25, μ and COP assume almost the same value. When the entrainment ratio is lower than 0.1, the system performance suffers an abrupt decrease, due to high primary mass flow rates $\dot{m}_{pf}$ (at the vapor generator) to satisfy the required low-pressure evaporator mass flow rate $\dot{m}_{ev}$. The detailed results of the thermodynamic analysis for each point of Figures 4 and 5 are reported in Appendix A for all the simulated combinations.

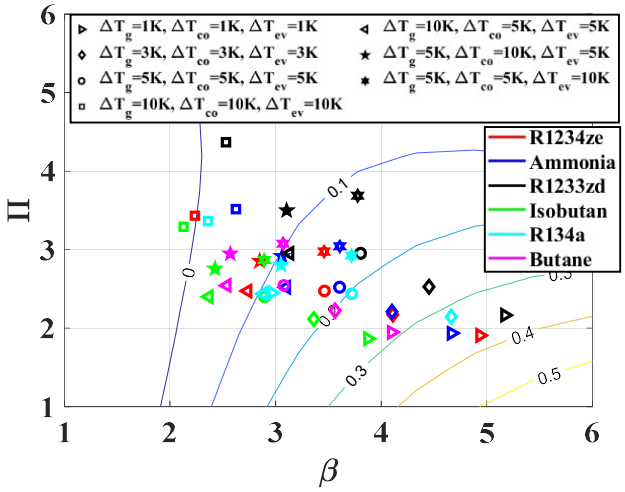

Figure 5. System COP (contour plot) as function of beta ratio and pressure lift for different pinch point values at the heat exchangers.

3. Thermo-Economic Analysis

The first part of this analysis proposes the calculation of the total investment costs (per unit cooling load) for each configuration in terms of working fluid, desired pinch points in the heat exchangers, and the efficiency of the regenerative heat exchanger. The results will be proposed in terms of conflicting goals: from one side the maximization of the system performance and from the other side the minimum specific investment cost, by therefore proposing an "optimum" configuration as reasonable compromise. The chosen solution will be then used in the second part of this section that analyzes an integrated system made up of a waste heat recovery hybrid ejector cycle (WHRHEC) working in parallel with a conventional vapor compression cycle (VCC), providing the minimum plant life that leads to an economic convenience.

3.1. Evaluation of the Heat Exchangers Surface

Dedicated heat transfer correlations were considered for each heat exchanger for the estimation of their heat transfer surface. According to the selected fluids properties, the high-pressure evaporator and the regenerative heat exchanger were designed to work in a range of pressures suitable for the use of plate heat exchangers, shell-and-tube type preferred because of their compactness. Considering the lower pressure levels, a one pass shell and tube heat exchanger was chosen for the low temperature evaporator. In this way, boiling takes place at the outer surface of the tube bundle and large pressure drops are therefore avoided. Finally, a fin and tube heat exchanger was chosen for the condenser, in which air was used as secondary fluid.

The overall heat transfer coefficient U (W m^{-2}K^{-1}) cannot be considered constant during the heat transfer process, especially in the single phase/two phase transition. For this reason, different sections for single-phase and two-phase were considered with appropriate heat transfer correlations. Each heat exchanger was divided into discrete elements having an elementary area dA, corresponding to an elementary length dz. With the assumption of heat exchanger adiabaticity through its surroundings, the heat transfer differential equation reads as:

$$\delta\dot{Q}(z) = U(z)dA \cdot [T_{hot}(z) - T_{cold}(z)]. \quad (6)$$

The temperature of the refrigerant T (K), was calculated with Refprop 9.0 software developed by NIST [30] using both the pressure and the enthalpy local value; the same process was used for the secondary fluid (water or air). The local enthalpies were integrated from the inlet of each heat exchanger, according to the energy balance reported in Equations (7) and (8):

$$h_{ref}(z+1) = h_{ref}(z) - \frac{d\dot{Q}}{\dot{m}_{ref}}, \quad (7)$$

$$h_f(z+1) = h_f(z) - \frac{d\dot{Q}}{\dot{m}_f}, \quad (8)$$

where the subscripts *ref* and *f* refer to the refrigerant and the secondary fluid side, respectively. The overall heat transfer coefficient U is computed with Equation (9) where, s is the thickness (m) of the tube or the plate and κ_{mat} is the material thermal conductivity (W m^{-1}K^{-1}). The convective heat transfer coefficient α (W m^{-2}K^{-1}) for both fluids can be evaluated with Equation (10), where κ_{fluid} is the fluid thermal conductivity (W m^{-1}K^{-1}).

$$U = \frac{1}{\frac{1}{\alpha_{ref}} + \frac{s}{\kappa_{mat}} + \frac{1}{\alpha_f}}, \quad (9)$$

$$\alpha = \frac{Nu \cdot \kappa_{fluid}}{D_h}. \quad (10)$$

A summary of the correlations for the Nusselt number Nu or the convective heat transfer coefficient for each heat exchanger geometry and for single-phase and two-phase heat transfer are reported in Table 3. The geometric elementary details are fixed for all the permuted solutions and are defined for each heat exchanger type in Appendix B.

Table 3. Single-phase and two-phase heat transfer correlations.

Single-Phase	Two-Phase
Plate heat exchanger	
Correlation of Martin [36] $Nu = 0.205\mathrm{Pr}^{\frac{1}{3}}\left(\frac{\mu_m}{\mu_w}\right)^{\frac{1}{6}}\left(fRe^2sin(2\beta)\right)^{0.374}$	Boiling heat transfer correlation of Park and Kim [37] $Nu = 12.47Re_{eq}^{0.33}Pr_l^{\frac{1}{3}}$
Shell and tube heat exchanger—shell side	
Correlation of McAdams [38] $Nu = 0.36\left(\frac{D_eG_s}{\mu}\right)^{0.55}\left(\frac{c_p\mu}{k}\right)^{\frac{1}{3}}\left(\frac{\mu}{\mu_w}\right)^{0.14}$	Pool boiling correlation of Cooper [39] $\alpha_{nb} = 55 \cdot pr^{0.12}(-0.4343log(pr))^{-0.55}M^{-0.5}q^{0.67}$
Shell and tube heat exchanger—tube side	
Correlation of Dittus-Boelter [40] $Nu = 0.023Re^{0.8}Pr^{0.4}$	-
Fin and tube heat exchanger	
Wang et al. [41] $J = 0.096 \cdot Re_{air}^{P3} \cdot N_R^{P4} \cdot \left(\frac{P_{fin}}{D_c}\right)^{P5} \cdot \left(\frac{P_{fin}}{D_h}\right)^{P6}\left(\frac{P_{fin}}{P_t}\right)^{-0.93}$ $\alpha_{air} = J \cdot \rho_{air} \cdot u_{air,max} \cdot c_{p,air} \cdot {Pr_{air}}^{-2/3}$	Condensation inside tubes, correlation of Shah [42] $Nu = 0.023Re^{0.8}Pr^{0.4}\left[(1-x)^{0.8} + \frac{3.8x^{0.76}\cdot(1-x)^{0.04}}{p_r^{0.38}}\right]$

An algorithm was developed and implemented in a Matlab code to obtain the surface of each heat exchanger. As an initial step, both the thermodynamic and geometric parameters were fixed. At

the first elementary section (z = 1), the local temperature of the working fluid was set equal to the temperature in points 2, 3, and 5 for the generator, evaporator, and condenser, respectively. The overall heat transfer coefficient U for each elementary volume was evaluated with the mentioned prediction methods as shown in Table 3. Then, the elementary heat power was obtained from Equation (6). By considering the heat exchanger adiabatic through its surroundings, the energy balances from Equations (7) and (8) allow the calculation of the specific enthalpies for the subsequent integration steps (z + 1). This procedure was repeated until the heat exchangers surface balances the required heat power. In this way, the total heat transfer surface A was then obtained for each investigated geometric configuration and boundary condition. The geometrical parameters fixed and to be calculated for each type of heat exchanger are specified in Appendix B.

3.2. Cost Functions

The set-up costs were calculated by considering the single cost of each component (working fluid pump, high-pressure evaporator, condenser, low-pressure evaporator, regenerative heat exchanger, and ejector), for which a cost correlation was used, as shown in Table 4. Specifically, an exponential expression [43] as a function of the sole nominal power was chosen for the pump price. The investment costs of the plate heat exchangers (high pressure evaporator and regenerative heat exchanger) and of the fin and tube condenser were obtained as a linear function of the total heat transfer surface, as suggested by [43,44]. The shell and tube low-pressure evaporator cost was taken from the work of Wildi-Tremblay and Grosselin [45], related to the total heat transfer surface with a power function. Since the ejector has to be designed ad-hoc for the specific application and cannot be treated as a commercial item, in this analysis the ejector cost was estimated as a linear function of the minimum required volume of a brass block from which the final ejector geometry is obtained through material removal processes (considering density of the brass ρ_{brass} of 8.73 kg cm^{-3} and specific cost c_{brass} of 4.85 € kg^{-1}). When using flammable working fluids, additional safety issues must be taken into account for electronic components: in this case an increasing of investment costs of +20% is considered for the condenser (due to the presence of Atex fan type required in the case of hazardous fluids) and pump. In addition, a corrective enhancement factor of 1.30 is instead considered when using ammonia, in order to take into account both toxicity and flammability issues.

Table 4. Cost functions for each component.

Components	Dependent Variable	Investment Costs IC (€)
Working fluid pump	Electrical power (W)	$IC_p = 900\left(\frac{W}{300}\right)^{0.25}$ [43]
High pressure evaporator	Heat exchanger surface (m^2)	$IC_{gv} = 190 + 310 \cdot A$ [43]
Low pressure evaporator	Heat exchanger surface (m^2)	$IC_{ev} = 3.28 \cdot 10^4\left(\frac{A}{80}\right)^{0.68}$ [45]
Condenser	Heat exchanger surface (m^2)	$IC_{co} = 25 \cdot A$ [44]
Regenerative heat exchanger	Heat exchanger surface (m^2)	$IC_{rhe} = 190 + 310 \cdot A$ [43]
Ejector	Minimum required volume of brass (cm^3)	$IC_{ej} = \rho_{brass} \cdot c_{brass} \cdot V$

3.3. Results and Discussion

The same boundary conditions concerning the cooling load, the secondary fluids temperatures, and the refrigerant thermodynamic constraints from Table 2 are still used for the thermo-economic analysis. The list of permuted parameters is instead provided in Table 5, by obtaining a total amount of 1500 simulation runs.

Table 5. Operating conditions used for the thermo-economic analysis.

Parameter	Range
Pinch points for the heat exchangers (°C)	1–10
Fluids	R1234ze, Ammonia, R1233zd(E), Isobutane, R134a, Butane
Regenerative heat exchanger efficiency	0.50–0.90

The complete set of solutions in terms of COP versus specific investment costs is shown in Figure 6. Each color refers to a working fluid, whereas the bigger markers correspond to the subset of solutions presented in the thermodynamic analysis (empty and full markers, respectively, for a regenerative heat exchanger efficiency of 0.90 and 0.50). Their shape is recalled in the legend and is related to specific pinch point values. All the remaining intermediate combinations are finally drawn with x-shaped markers.

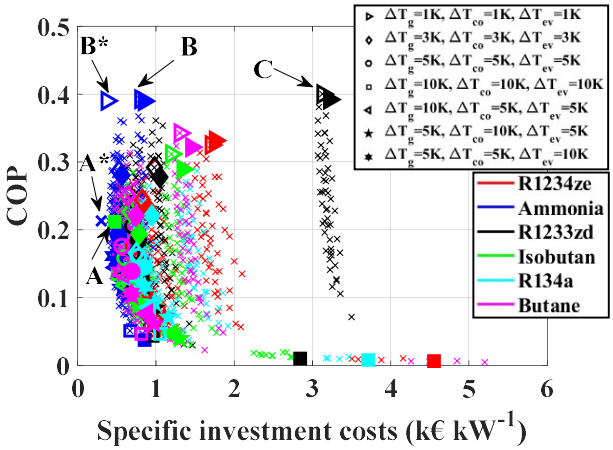

Figure 6. COP versus specific investment costs for all the chosen combinations. The highlighted markers refer to the solutions investigated for the thermodynamic analysis and each color is related to a specific working fluid.

By increasing the pinch point values, the performance decreases as already shown in the thermodynamic analysis. The effect of a different minimum temperature difference on the specific investment costs is, however, not univocal. From one side, higher pinch point values lead to lower heat exchanger efficiency that are therefore more compact (and cheaper). From the other side, the entrainment ratio μ decreases dramatically with an increasing pinch point (see Figure 4), leading to a lower entrained mass flow rate and therefore higher thermal loads at the high-pressure evaporator and condenser in order to satisfy the required cooling load, resulting in increased heat transfer surfaces and costs.

Regarding the refrigerant effect, although economically penalized by toxicity and flammability issues, the investigated solutions using ammonia as working fluid are those falling in the lowest specific investment cost region, due to a very high latent heat and its particularly favorable thermodynamic and transport properties for two-phase heat transfer. The opposite situation is observed for the synthetic refrigerant R1233zd(E), that presents higher specific set-up costs with respect to other refrigerants when the same boundary conditions are applied. For the present analysis, three singular solutions (namely A, B, and C), chosen as possible "optimum" cases, are extracted from the total set of simulations and the related main parameters are summarized in Table 6. The share of the total investment costs for these configurations is specified in Figure 7. Specifically, solution A provides the plant configuration with the lowest specific investment cost of 0.40 k€ per kW of cooling load. Almost half of the entire cost (42%) is related to the high-pressure evaporator, followed by the low-pressure evaporator (32%),

the electric pump (17%), and the fin and tube condenser (4%). This configuration uses ammonia as refrigerant, with a pinch point of 1 °C at the condenser, with a minimum temperature difference of 7 and 10 °C in high- and low-pressure evaporator, respectively, and an efficiency of the regenerative heat exchanger of 0.50. The related COP is however low (0.21) caused by a reduced entrainment ratio of 0.227. From another perspective, solution C maximizes the system performance, with a COP of 0.40, using R1233zd(E) as refrigerant, all the minimum temperature differences set to 1 °C, and the internal heat exchanger efficiency of 0.50. In contrast, the specific set-up cost is very high (3.13 k€ kW^{-1}), due to the penalized heat transfer efficiency for this low reduced-pressure fluid, that leads to large required heat transfer surfaces. In fact, approximately 99% of the total specific costs are attributed to the heat exchangers (see Figure 7). Finally, solution B represents the reasonable trade-off between low investment costs and high system performance. The corresponding set-up cost is 0.80 k€ kW^{-1}, significantly lower than that of solution C, with only a slight penalization on the COP value, equal to 0.39. For this configuration, ammonia is the working fluid and all the pinch point values are set to 1 °C, with an efficiency of the internal plate heat exchanger equal to 0.50.

Table 6. Summary of the three configurations chosen as possible optimum case. The asterisk solutions refer to the use of a plate heat exchanger instead of a shell and tube heat exchanger for the low-pressure evaporator.

	Fluid	ΔT_{gv} (°C)	ΔT_{co} (°C)	ΔT_{ev} (°C)	ε_{RHE} (-)	Tgv (°C)	Pgv (bar)	Tco (°C)	Pco (bar)	Tev (°C)	Pev (bar)	μ (-)	Π (-)	β (-)	COP (-)	ic (k€ kW^{-1})
A/A *	R717	7	1	10	0.50	80.2	41.6	25.8	10.3	–3.0	3.8	0.227	2.69	4.04	0.21	0.40/0.30 *
B/B *	R717	1	1	1	0.50	88.3	49.4	25.9	10.3	6.0	5.3	0.407	1.93	4.79	0.39	0.80/0.37 *
C	R1233zd	1	1	1	0.50	87.9	7.93	25.6	1.32	6.0	0.62	0.497	2.13	5.99	0.40	3.13

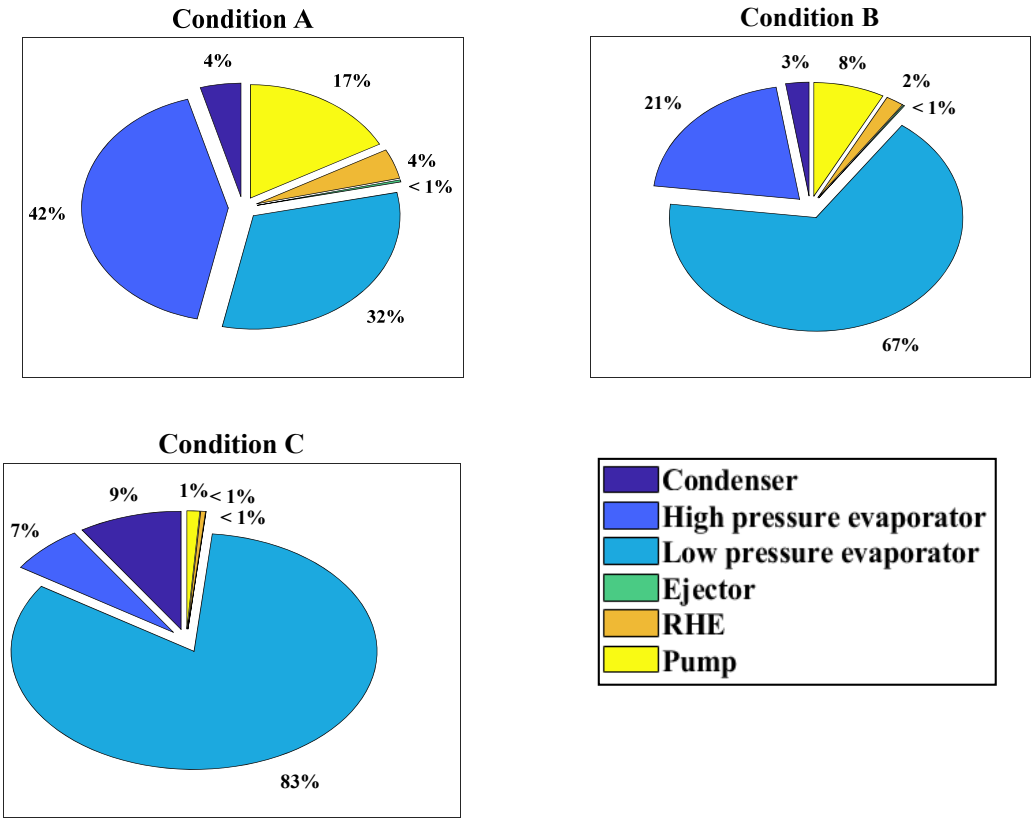

Figure 7. Share of the total investment costs for the hybrid ejector plant.

It is worth highlighting that the same heat exchanger typologies were selected for all fluids to preserve the analysis consistency. However, the higher evaporating pressures obtained for fluids having a high p-t saturation curve (as ammonia) may allow the use of a plate heat exchanger as

low-pressure evaporator instead of a shell and tube heat exchanger. This would strongly reduce the set-up costs associated to this component (up to 80%) and increase the system compactness as well. Solutions A* and B* in Figure 6 and in Table 6 therefore refer to the corresponding simulations A and B, in which the low-pressure evaporator is replaced by a cheaper plate heat exchanger.

It is important to remark that the best design option is a matter of choice, once the desired criterion and potential further constraints are established (minimum cost—maximum performance—avoiding toxic and/or flammable refrigerants, etc.). The discussion regarding the rationale used to define the best configuration is therefore case-sensitive and is not included in the scope of this paper.

Finally, the investment cost-performance map obtained in Figure 6 is placed together with the corresponding maps of existing waste heat driven technologies for cooling purposes in Figure 8. It is shown that the WHRHEC systems provide similar thermodynamic COPs and lower set-up costs with respect to ORC/VCC combined plants. Regarding the comparison with single-effect absorption chillers, WHRHEC systems provide lower COP at the same costs. It is worth noting, however, that the declared performances of the consolidated technologies (as shown in the introductive section), even if falling in the same operative ranges of Table 2, are related to large plant sizes and cooling loads (>100 kW), whereas the set-up costs of WHRHEC systems are likely not to be influenced by size effects.

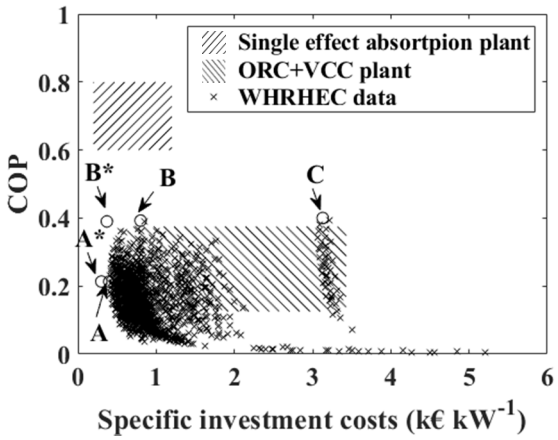

Figure 8. System performance and specific investment costs range of organic Rankine cycle (ORC) + vapor compression cycle (VCC) and single effect absorption plant. Highlighted solutions: A (minimum cost), C (maximum performance), and B (best compromise between cost and COP). Asterisk solutions A * and B * refer to plate heat exchanger type at the low-pressure evaporator instead of a shell and tube heat exchanger.

3.4. Total Costs Analysis for VCC Integrated User

The configuration B was finally used to analyze the economic advantage of a waste heat recovery hybrid ejector cycle (WHRHEC) with respect to a typical vapor compression cycle (VCC). In particular, the analysis was focused on an end user with a required cooling load $\dot{Q}_{ev,USER}$, supplied by having both WHRHEC (size $\dot{Q}_{ev,WHR}$) and a VCC (size $\dot{Q}_{ev,VCC}$) working in parallel, as shown in the schematic example of Figure 9. The aim of this preliminary economic analysis was to define a method able to establish the required lifetime of the combined WHR/VCC system that leads to an economic convenience, once design and contingent parameters, such as the availability of the waste heat source, the specific cost of electric energy, and the size of the WHR plant, were fixed. The WHRHEC being a brand new technology among the possible waste heat recovery solutions, its space in the marketplace is still absent or very limited, leading to an indetermination of several mentioned economic terms such as maintenance costs and investment depreciation.

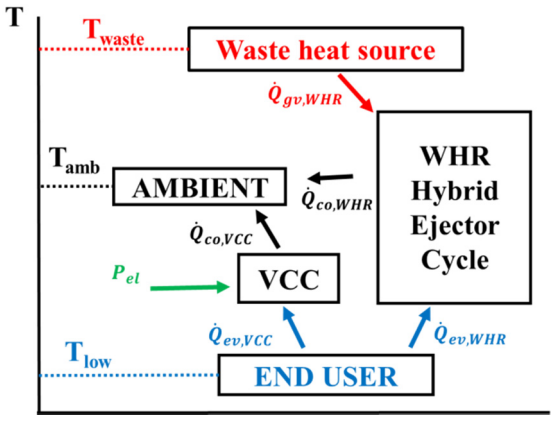

Figure 9. Schematic diagram of a combined waste heat recovery hybrid ejector cycle (WHRHEC)/VCC system to supply the end user cooling load.

The total costs TC of the integrated WHR/VCC plant for its entire lifetime $\Delta\theta_{LIFE}$ include the investment costs of both systems and the running costs of the VCC plant due to the electrical energy consumption E_{el}. No running costs are here considered for the WHRHEC system, by keeping the hypothesis of free-of-charge availability of the waste heat.

$$TC = \dot{Q}_{ev,WHR} k_{WHR} + \dot{Q}_{ev,VCC} k_{VCC} + E_{el}\, k_{ee}. \tag{11}$$

In Equation (11), k_{WHR} and k_{VCC} are the set-up specific costs (k€ kW^{-1}) of the WHR and the VCC plant, respectively. Particularly, k_{WHR} refers to the optimal solution B of the previous section and is therefore considered equal to 0.80 k€ kW^{-1} in the present analysis. $\dot{Q}_{ev,WHR}$ and $\dot{Q}_{ev,VCC}$ are the cooling capacities of the two systems, whereas κ_{ee} is the specific cost of electric energy (k€ kWh^{-1}). The VCC plant is most likely designed to fulfill the entire cooling load, in order to satisfy the user requirements also when the waste heat recovery mode is not available. The parameter X_{WHR} defines instead the fraction of the cooling load covered by the WHR plant.

$$\dot{Q}_{ev,VCC} = \dot{Q}_{ev,user}, \tag{12}$$

$$X_{WHR} = \frac{\dot{Q}_{ev,WHR}}{\dot{Q}_{ev,user}}. \tag{13}$$

The electric energy consumption $E_{el}E_{el}$ in the system lifetime $\Delta\theta_{LIFE}$ is then required only when the waste heat recovery system is not used and is a function of the seasonal COP ($SCOP$) of the VCC cycle. By defining $\Delta\theta_{WHR}$ as the period of the lifetime in which the waste heat source is available, the electric consumption reads as:

$$E_{el} = \frac{Q_{ev,VCC}}{SCOP} = \frac{Q_{ev,user} - Q_{ev,WHR}}{SCOP} = \frac{\dot{Q}_{ev,user}\Delta\theta_{LIFE} - \dot{Q}_{ev,user} X_{WHR}\Delta\theta_{WHR}}{SCOP}. \tag{14}$$

To make the saving costs not depend on the plant size, the total costs are divided by the heat load: in this way, once obtained the specific savings, they have a more general meaning and are not related to a specific size. The total specific costs per unit of cooling load tc (k€ kW^{-1}) can be therefore expressed by Equation (15), in which Y is the fraction of the total lifetime period when the waste heat source is available, as for Equation (16).

$$tc = \frac{TC}{\dot{Q}_{ev,user}} = X_{WHR} k_{WHR} + k_{VCC} + \frac{\Delta\theta_{LIFE}}{SCOP}(1 - X_{WHR} Y) k_{ee}, \tag{15}$$

$$Y = \frac{\Delta\theta_{WHR}}{\Delta\theta_{LIFE}}. \tag{16}$$

Finally, Equation (17) provides the specific cost savings with respect to a simple configuration in which the WHRHEC is not considered and only the VCC plant fulfills the cooling load requirements ($X_{WHR} = 0$):

$$\Delta tc = X_{WHR}\left(\frac{\Delta\theta_{LIFE}}{SCOP} \cdot Y \cdot k_{ee} - k_{WHR}\right). \tag{17}$$

Figure 10a shows the cost savings Δtc as a function of the total lifetime of the combined system for different values of the parameter X_{WHR}. The fraction of the waste heat availability Y is fixed at 80%, whereas the Italian cost of the electric energy [44] and a *SCOP* value of 2.5 are considered. It is worth noting that the size of the WHR plant does not influence the even point (zero-saving), approximately reached after almost 2 years (by considering 4000 h of operation per year) within these hypotheses. A higher X_{WHR} leads however to higher savings after the even point and to higher losses for plants dismantled before the zero-saving time is reached. The effect of the waste heat availability Y for a fixed size of the WHR plant ($X_{WHR} = 0.5$) is shown in Figure 10b. The economic convenience is more and more anticipated for higher waste heat availabilities. However, when is too low (e.g., 20%), the even point can be never reached in a reasonable lifetime (10 years).

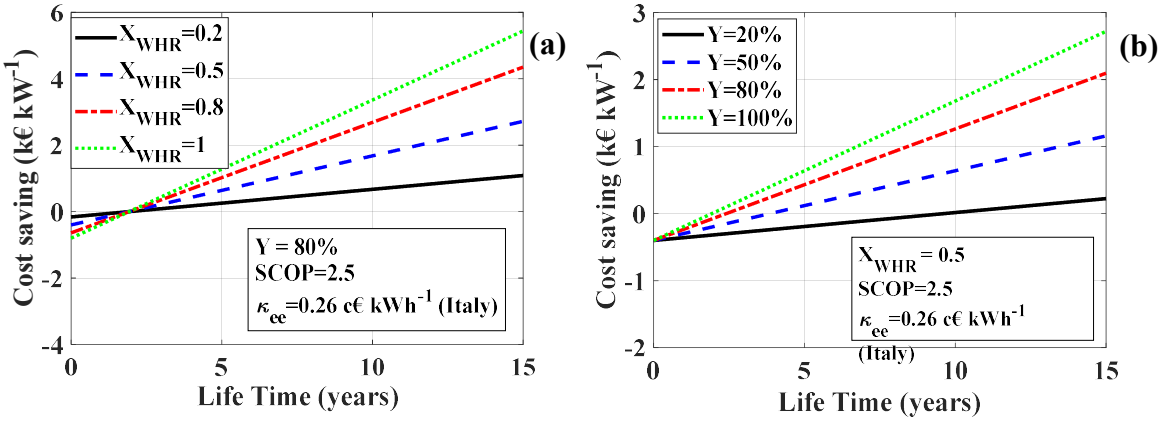

Figure 10. Specific cost savings as a function of the operating time of the combined plant (4000 working hours per year are considered). Seasonal COP (SCOP) and κ_{ee} are, respectively, fixed to 2.5 and 0.26 c€ kWh^{-1} (Italian market [46]). (**a**) Effect of the WHR plant size for $Y = 0.80$; (**b**) effect of the waste heat availability for $X_{WHR} = 0.5$.

Figure 11 shows the required operating time to reach the even point (Δtc = 0) as a function of the waste heat utilization Y, with each curve referring to a different specific cost of energy κ_{ee} [46]. For the Italian market, by considering a realistic lifetime of 7 years, the use of a WHRHEC/VCC integrated system would be economically convenient only if the availability of the heat source overcomes 28% (approximately 7800 h) of the entire operating period. Higher values of Y are instead required in countries where the electric energy is cheaper (as France, with κ_{ee} equal to 0.18 c€ kWh^{-1}).

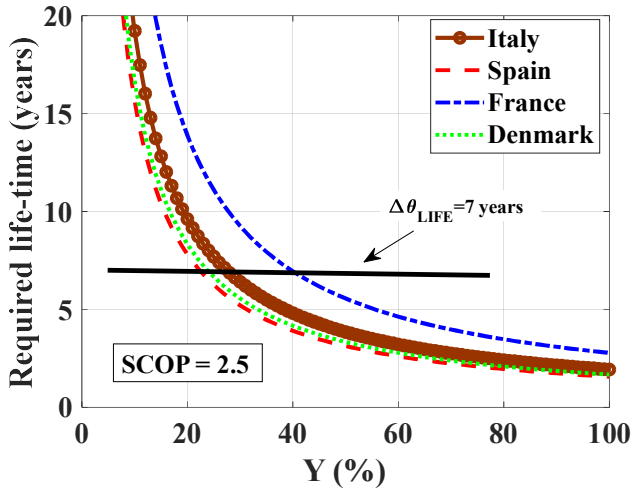

Figure 11. Required lifetime (Δtc = 0) as a function of the waste heat availability *Y*, for different countries according to their specific cost of the electric energy. The horizontal line refers to a realistic operating time of 7 years.

Finally, Figure 12 presents the WHR size (X_{WHR})—waste heat availability (*Y*) for the Italian market and an operating overall lifetime of 7 years, highlighting both loss and saving regions. As shown, the even point is reached for *Y* equal to 28% at any size of the WHR plant. For higher waste heat utilizations, the blue curves provide the specific savings, increasing with both WHR size and *Y*. Similarly, in the left zone the red curves show the specific losses, increasing with greater WHR size and lower waste heat availability.

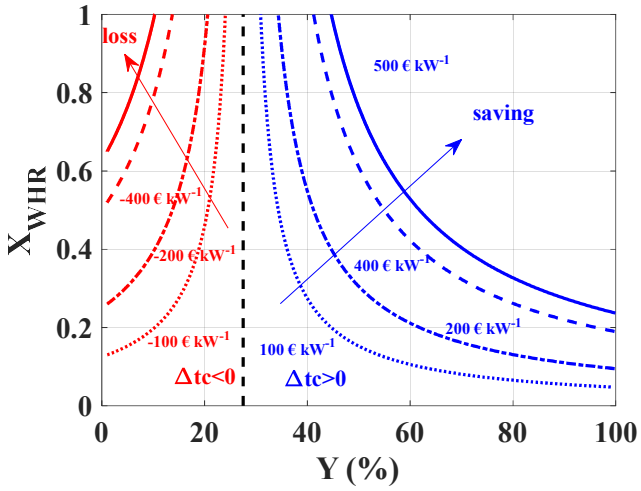

Figure 12. X_{WHR}-*Y* map developed for the Italian cost of the electric energy, by considering a total operating time of 7 years and a *SCOP* of the VCC plant equal to 2.5. The curves refer to either specific cost savings (in blue) or losses (in red).

4. Conclusions

A thermo-economic analysis of a waste heat recovery hybrid ejector cycle (WHRHEC) for air conditioning purposes was performed in this paper. The thermodynamic performances and the specific set-up costs were evaluated for different plant configurations in terms of working fluids and pinch point values at the heat exchangers, in order to place the WHRHEC systems among the actual heat driven cooling technologies available on the market. The peculiar simulation results, A (minimum investment costs), C (maximum thermodynamic COP), and B (chosen trade-off between maximum performance and minimum cost) are highlighted in Figure 8. The following economic analysis will give

the reader a realistic order of magnitude about the economic convenience in the use of the WHRHEC systems instead of traditional vapor compression cycles, when a certain amount of waste heat is available. The main outcomes of this study may be summarized as follows:

- WHRHEC solutions employing ammonia are the most performing and also economically advantageous cases, due to the ammonia high latent heat and favorable thermodynamic and transport properties during two-phase heat transfer. Moreover, the higher low-temperature evaporating pressures may allow the use of a cheaper and more compact plate heat exchanger instead of a tube and shell low-temperature evaporator, thus further reducing the set-up costs (solutions A* and B*).
- The cost-performance comparison with existing waste heat driven technologies for cooling purposes shows that the WHRHEC systems provide similar performances and lower investment costs with respect to ORC/VCC combined plants; instead WHRHEC systems give lower COP values at the same costs of single-effect absorption chillers. However, the declared performances of the consolidated technologies are related to large plant sizes and cooling loads (>100 kW), while costs of WHRHEC systems is not affected by size effects.
- The economic analysis has shown that a WHRHEC may be a convenient solution to be integrated with a conventional VCC system in a plant according to the specific cost of electric energy and the waste heat time availability. Specifically, for the Italian situation, by considering a total lifetime of 28,000 h (7 years and 4000 h per year of operation), the economical convenience of the WHRHEC system is reached when the waste heat exploitation overcomes approximately 7800 h (28% of the entire lifetime). Higher (lower) waste-heat availability periods are instead required where the cost of electric energy is lower (higher), as in France (40%) (as in Spain, 24% and Denmark, 26%).

Author Contributions: Conceptualization, A.W.M.; Data curation, G.L.; Funding acquisition, R.M.; Methodology, A.W.M.; Supervision, A.W.M.; Writing—original draft preparation, L.V.; Writing—review & editing, R.T. All authors have read and agreed to the published version of the manuscript.

Funding: This research was funded by "Ministero dell'Istruzione dell'Università e della Ricerca" via the project PRIN2015 "Clean Heating and Cooling Technologies for an Energy Efficient Smart Grid", which is gratefully acknowledged.

Conflicts of Interest: The authors declare no conflict of interest.

Nomenclature

A	heat exchanger surface (m^2)	*Greek*	
A_r	ejector area ratio (m^2)	α	convective heat transfer coefficient (W m^{-2} K^{-1})
c_p	specific heat at constant pressure (kJ kg^{-1} K^{-1})	β	ejector beta ratio
COP	coefficient of performance	Δ	difference
D	diameter (m)	ε	heat exchanger efficiency
E_{el}	electrical energy consumption (kJ)	η	efficiency
GWP	global warming potential ($kgCO_{2eq}$ kg^{-1})	θ	time
h	specific enthalpy (kJ kg^{-1})	κ	thermal conductivity [W m^{-1} K^{-1})
ic	specific investment costs (k€ kW^{-1})	κ_{ee}	specific cost of electric energy (€ kWh^{-1})
IC	investment costs (k€)	μ	entrainment ratio
k	heat capacity ratio	Π	pressure lift
k_{vcc}	Set-up specific cost VCC (k€ kW^{-1})	*Subscripts*	
k_{WHR}	Set-up specific cost WHR (k€ kW^{-1})	air	related to the air
G	mass flux (kg s^{-1} m^{-2})	co	condenser
	mass flow rate (kg s^{-1})	cold	cold side
N	number of elements	cr	critical condition
Nu	Nusselt number	D	diffuser
ODP	ozone depletion potential	ev	evaporator
ORC	organic Rankine cycle	f	secondary fluid

P	pressure (bar)	fin	fin
Pr	Prandtl number	fluid	related to the fluid
$\dot{Q}$	heat capacity (kW)	h	hydraulic
R	ideal gas constant (kJ kg^{-1} K^{-1})	hot	hot side
Re	Reynolds number	M	mixing chamber
s	tube thickness (m)	m	mixing section
SCOP	seasonal coefficient of performance	mat	material
T	temperature (K)	N	motive nozzle
tc	specific total costs (k€ kW^{-1})	nb	nucleate boiling contribution
TC	total costs (k€)	pf	primary flow
u	velocity (m s^{-1})	R	rank
U	overall heat transfer coefficient (W m^{-2} K^{-1})	ref	related to the refrigerant
V	volume (m^3)	rhe	regenerative heat exchanger
VCC	vapor compression cycle	s	isentropic
W	power consumption (kW)	sf	secondary flow
WHRHEC	waste heat recovery hybrid ejector cycle	t	motive nozzle throat section
X_{WHR}	fraction of the cooling load covered by the WHR plant	tp	two−phase
Y	fraction of the total lifetime period when the waste heat source is available	vg	vapor generator
		WHR	waste heat recovery

Appendix A. Thermodynamic Analysis Results

Table A1. Thermodynamic analysis results for R1234ze.

R1234ze														
ΔT_{gv} (°C)	ΔT_{co} (°C)	ΔT_{ev} (°C)	T_{gv} (°C)	P_{gv} (bar)	T_{co} (°C)	P_{co} (bar)	T_{ev} (°C)	P_{ev} (bar)	μ (-)	Π (-)	β (-)	COP (-)	Q_{gv} (kW)	Q_{co} (kW)
1	1	1	91.1	25.3	25.8	5.1	6	2.7	0.370	1.90	4.95	0.33	60.0	80.9
3	3	3	85.0	22.33	27.9	5.43	4	2.50	0.261	2.17	4.11	0.23	86.6	107.6
5	5	5	79.7	19.95	29.9	5.76	2	2.33	0.173	2.47	3.46	0.15	133.0	154.4
10	5	5	69.0	15.75	29.9	5.76	2	2.33	0.096	2.47	2.73	0.08	237.0	258.7
5	10	5	77.3	18.95	34.9	6.65	2	2.33	0.084	2.85	2.85	0.07	279.7	302.3
5	5	10	79.7	19.94	29.9	5.76	−3	1.94	0.140	2.98	3.46	0.12	168.0	189.7
10	10	10	66.5	14.86	34.8	6.65	−3	1.94	0.008	3.43	2.24	0.01	3168.4	3208.4

Table A2. Thermodynamic analysis results for Ammonia.

Ammonia														
ΔT_{gv} (°C)	ΔT_{co} (°C)	ΔT_{ev} (°C)	T_{gv} (°C)	P_{gv} (bar)	T_{co} (°C)	P_{co} (bar)	T_{ev} (°C)	P_{ev} (bar)	μ (-)	Π (-)	β (-)	COP (-)	Q_{gv} (kW)	Q_{co} (kW)
1	1	1	87.2	48.3	25.9	10.3	6	5.3	0.397	1.93	4.68	0.39	51.1	71.5
3	3	3	83.9	45.06	28.0	10.98	4	4.97	0.286	2.21	4.10	0.28	71.3	91.8
5	5	5	80.7	42.04	30.0	11.66	2	4.62	0.197	2.52	3.61	0.19	104.1	124.8
10	5	5	73.8	36.13	29.9	11.65	2	4.62	0.132	2.52	3.10	0.13	156.0	176.8
5	10	5	79.9	41.30	34.9	13.49	2	4.62	0.108	2.92	3.06	0.11	189.7	210.8
5	5	10	80.7	42.05	30.0	11.66	−3	3.83	0.159	3.04	3.61	0.15	129.8	150.6
10	10	10	72.9	35.36	34.9	13.48	−3	3.83	0.039	3.52	2.62	0.04	534.4	556.9

Table A3. Thermodynamic analysis results for R1233zd.

R1233zd														
ΔT_{gv} (°C)	ΔT_{co} (°C)	ΔT_{ev} (°C)	T_{gv} (°C)	P_{gv} (bar)	T_{co} (°C)	P_{co} (bar)	T_{ev} (°C)	P_{ev} (bar)	μ (-)	Π (-)	β (-)	COP (-)	Q_{gv} (kW)	Q_{co} (kW)
1	1	1	82.2	6.9	25.9	1.3	6	0.6	0.438	2.16	5.19	0.39	50.8	70.9
3	3	3	78.9	6.41	27.9	1.44	4	0.57	0.313	2.53	4.45	0.28	72.0	92.3
5	5	5	75.4	5.87	29.9	1.54	2	0.52	0.210	2.95	3.81	0.18	108.4	128.7
10	5	5	67.8	4.83	29.9	1.54	2	0.52	0.151	2.95	3.13	0.13	150.7	171.0
5	10	5	74.1	5.67	34.9	1.83	2	0.52	0.098	3.50	3.11	0.08	237.2	257.7
5	5	10	75.1	5.83	29.9	1.54	−3	0.42	0.130	3.69	3.78	0.11	178.4	198.8
10	10	10	66.2	4.62	34.9	1.83	−3	0.42	0.012	4.37	2.53	0.01	1957.0	1980.4

Table A4. Thermodynamic analysis results for Isobutan (R600a).

Isobutano														
ΔT_{gv} (°C)	ΔT_{co} (°C)	ΔT_{ev} (°C)	T_{gv} (°C)	P_{gv} (bar)	T_{co} (°C)	P_{co}(bar)	T_{ev}(°C)	P_{ev} (bar)	μ (-)	Π (-)	β (-)	COP (-)	Q_{gv} (kW)	Q_{co} (kW)
1	1	1	81.9	14.0	25.9	3.6	6	1.9	0.322	1.86	3.88	0.29	68.8	89.4
3	3	3	77.8	12.83	27.9	3.82	4	1.80	0.218	2.12	3.36	0.19	103.3	124.0
5	5	5	73.4	11.70	29.9	4.04	2	1.68	0.132	2.40	2.90	0.12	173.1	194.1
10	5	5	64.2	9.57	29.9	4.04	2	1.68	0.053	2.40	2.37	0.05	425.3	447.2
5	10	5	71.6	11.25	34.9	4.64	2	1.68	0.046	2.76	2.42	0.04	503.0	525.7
5	5	10	73.4	11.69	29.9	4.04	−3	1.41	0.107	2.87	2.89	0.09	218.4	239.7
10	10	10	65.6	9.88	34.9	4.64	−3	1.41	0.261	3.29	2.13	0.21	94.4	114.8

Table A5. Thermodynamic analysis results for R134a.

R134a														
ΔT_{gv} (°C)	ΔT_{co} (°C)	ΔT_{ev} (°C)	T_{gv} (°C)	P_{gv} (bar)	T_{co} (°C)	P_{co} (bar)	T_{ev} (°C)	P_{ev} (bar)	μ (-)	Π (-)	β (-)	COP (-)	Q_{gv} (kW)	Q_{co} (kW)
1	1	1	82.1	26.3	25.8	6.8	6	3.6		1.88	3.86			
3	3	3	92.0	33.78	27.9	7.24	4	3.38	0.242	2.14	4.66	0.22	90.5	112.1
5	5	5	83.8	28.54	29.9	7.67	2	3.15	0.161	2.44	3.72	0.14	138.0	159.9
10	5	5	71.9	22.08	29.8	7.67	2	3.15	0.095	2.44	2.88	0.09	233.7	255.9
5	10	5	81.1	26.94	34.8	8.83	2	3.15	0.081	2.81	3.05	0.07	280.9	304.5
5	5	10	83.8	28.53	29.9	7.67	−3	2.62	0.132	2.92	3.72	0.12	171.6	194.0
10	10	10	69.3	20.82	34.8	8.83	−3	2.62	0.009	3.37	2.36	0.01	2471.2	2511.9

Table A6. Thermodynamic analysis results for Butane (R600).

Butane														
ΔT_{gv} (°C)	ΔT_{co} (°C)	ΔT_{ev} (°C)	T_{gv} (°C)	P_{gv} (bar)	T_{co} (°C)	P_{co} (bar)	T_{ev} (°C)	P_{ev} (bar)	μ (-)	Π (-)	β (-)	COP (-)	Q_{gv} (kW)	Q_{co} (kW)
1	1	1	80.7	10.3	26.0	2.5	6	1.3	0.356	1.95	4.10	0.32	62.1	82.5
3	3	3	77.1	9.49	27.9	2.66	4	1.20	0.248	2.22	3.56	0.22	90.6	111.0
5	5	5	73.2	8.71	29.9	2.83	2	1.11	0.158	2.54	3.08	0.14	144.0	164.5
10	5	5	64.9	7.18	30.0	2.83	2	1.11	0.086	2.54	2.54	0.08	262.4	283.2
5	10	5	71.8	8.43	34.9	3.28	2	1.11	0.071	2.95	2.57	0.06	325.7	346.8
5	5	10	73.2	8.69	29.9	2.83	−3	0.92	0.125	3.08	3.07	0.11	186.2	206.9
10	10	10	47.4	4.63	35.9	3.37	−3	0.92	-0.121	3.66	1.37			

Appendix B. Heat Exchangers Geometrical Data

Table A7. Main sizing parameters of the heat exchangers.

High Pressure Evaporator Plate Heat Exchanger		**Condenser Plate Fin and Tube**		**Low Pressure Evaporator One Pass Shell and Tube**	
Plate height (mm)	To calculate	Tube length (mm)	to calculate	Tube length (mm)	To calculate
Plate width (mm)	500	Fin step (mm)	2.5	Tube number	To calculate
Plate spacing (mm)	1.0	Fin thickness (mm)	0.3	Internal tube diameter (mm)	12
Wavelength corrugation (mm)	1.0	Tube step (mm)	33	Tube thickness (mm)	0.5
Chevron angle (°)	80	Rank step (mm)	33	Pitch size (mm)	18
Channel number (#)	10	Tube number (#)	10	Baffle spacing (mm)	160
Plate thickness (mm)	0.2	Tube external diameter (mm)	10	Shell diameter (mm)	180
		Tube thickness (mm)	1.0		
		Rank number (#)	5		

References

1. IEA. *The Future of Cooling*; IEA: Paris, France, 2018; Available online: https://www.iea.org/reports/the-future-of-cooling (accessed on 22 January 2020).
2. Mapping and Analysis of the Current and Future (2020–2030) heating/cooling fuel deployment (fossils/renewables). Fraunhofer and alia; Publisher: Place of Publication, March. 2016. Available online: https://ec.europa.eu/energy/sites/ener/files/documents/Report%20WP1.pdf (accessed on 22 January 2020).
3. Henning, H.M. Solar assisted air conditioning of buildings–An overview. *Appl. Therm. Eng.* **2007**, *27*, 1734–1749. [CrossRef]
4. Baniyounes, A.M.; Ghadi, Y.Y.; Rasul, M.G.; Khan, M.M.K. An overview of solar assisted air conditioning in Queensland's subtropical regions, Australia. *Renew. Sustain. Energy Rev.* **2013**, *26*, 781–804. [CrossRef]
5. Güido, W.H.; Lanser, W.; Petersen, S.; Ziegler, F. Performance of absorption chillers in field tests. *Appl. Therm. Eng.* **2018**, *134*, 353–359. [CrossRef]
6. *Meeting Cooling Demands in Summer by Applying Heat from Cogeneration*; Summerheat Publishable Report; Berliner Energieagentur GmbH: Berlin, Germany, 2009; Available online: https://www.euroheat.org/wp-content/uploads/2016/04/SUMMERHEAT_Report.pdf (accessed on 22 January 2020).
7. Hassan, H.Z.; Mohamad, A.A. A review on solar-powered closed physisorption cooling systems. *Renew. Sustain. Energy Rev.* **2012**, *16*, 2516–2538. [CrossRef]
8. Ferreira, C.I.; Kim, D.S. Techno-economic review of solar cooling technologies based on location-specific data. *Int. J. Refrig.* **2014**, *39*, 23–37. [CrossRef]
9. Zhai, X.Q.; Qu, M.; Li, Y.; Wang, R.Z. A review for research and new design options of solar absorption cooling systems. *Renew. Sustain. Energy Rev.* **2011**, *15*, 4416–4423. [CrossRef]
10. Quoilin, S.; Van Den Broek, M.; Declaye, S.; Dewallef, P.; Lemort, V. Techno-economic survey of Organic Rankine Cycle (ORC) systems. *Renew. Sustain. Energy Rev.* **2013**, *22*, 168–186. [CrossRef]
11. Aphornratana, S.; Sriveerakul, T. Analysis of a combined Rankine–vapour–compression refrigeration cycle. *Energy Convers. Manag.* **2010**, *51*, 2557–2564. [CrossRef]
12. Tocci, L.; Pal, T.; Pesmazoglou, I.; Franchetti, B. Small scale organic rankine cycle (ORC): A techno-economic review. *Energies* **2017**, *10*, 413. [CrossRef]
13. Secretariat, O. *Handbook for the Montreal Protocol on Substances that Deplete the Ozone Layer*; UNEP: Nairobi, Kenya, 2006; pp. 1–743.
14. The European Parliament and the Council of the European Union. Regulation (EU) No. 517/2014 of the European Parliament and of the Council of 16 April 2014 on fluorinated greenhouse gases and repealing Regulation (EC) No. 842/2006. *Off. J. Eur. Union* **2014**, *L150*, 195–230.
15. Tashtoush, B.; Alshare, A.; Al-Rifai, S. Performance study of ejector cooling cycle at critical mode under superheated primary flow. *Energy Convers. Manag.* **2015**, *94*, 300–310. [CrossRef]

16. Hernandez, J.I.; Roman, R.; Best, R.; Dorantes, R.; Gonzalez, H.E. The behavior of an ejector cooling system operating with refrigerant blends 410A and 507. *Energy Procedia* **2014**, *57*, 3021–3030. [CrossRef]
17. Chen, J.; Jarall, S.; Havtun, H.; Palm, B. A review on versatile ejector applications in refrigeration systems. *Renew. Sustain. Energy Rev.* **2015**, *49*, 67–90. [CrossRef]
18. Besagni, G.; Mereu, R.; Inzoli, F. Ejector refrigeration: A comprehensive review. *Renew. Sustain. Energy Rev.* **2016**, *53*, 373–407. [CrossRef]
19. Butrymowicz, D.; Śmierciew, K.; Karwacki, J.; Gagan, J. Experimental investigations of low-temperature driven ejection refrigeration cycle operating with isobutane. *Int. J. Refrig.* **2014**, *39*, 196–209. [CrossRef]
20. Besagni, G.; Mereu, R.; Di Leo, G.; Inzoli, F. A study of working fluids for heat driven ejector refrigeration using lumped parameter models. *Int. J. Refrig.* **2015**, *58*, 154–171. [CrossRef]
21. Zegenhagen, M.T.; Ziegler, F. Experimental investigation of the characteristics of a jet-ejector and a jet-ejector cooling system operating with R134a as a refrigerant. *Int. J. Refrig.* **2015**, *56*, 173–185. [CrossRef]
22. Wang, H.; Cai, W.; Wang, Y.; Yan, J.; Wang, L. Experimental study of the behavior of a hybrid ejector-based air-conditioning system with R134a. *Energy Convers. Manag.* **2016**, *112*, 31–40. [CrossRef]
23. Dahmani, A.; Aidoun, Z.; Galanis, N. Optimum design of ejector refrigeration systems with environmentally benign fluids. *Int. J. Therm. Sci.* **2011**, *50*, 1562–1572. [CrossRef]
24. Gil, B.; Kasperski, J. Efficiency analysis of alternative refrigerants for ejector cooling cycles. *Energy Convers. Manag.* **2015**, *94*, 12–18. [CrossRef]
25. Chen, J.; Havtun, H.; Palm, B. Screening of working fluids for the ejector refrigeration system. *Int. J. Refrig.* **2014**, *47*, 1–14. [CrossRef]
26. Śmierciew, K.; Gagan, J.; Butrymowicz, D.; Łukaszuk, M.; Kubiczek, H. Experimental investigation of the first prototype ejector refrigeration system with HFO-1234ze (E). *Appl. Therm. Eng.* **2017**, *110*, 115–125. [CrossRef]
27. Atmaca, A.U.; Erek, A.; Ekren, O. Investigation of new generation refrigerants under two different ejector mixing theories. *Energy Procedia* **2017**, *136*, 394–401. [CrossRef]
28. Björn, P. *R1336mzz-Z—New Generation Nonflammable Low GWP Refrigerant*; Department of Energy Technology, Royal Institute of Technology: Stockholm, Sweden, 2014.
29. Honeywell Refrigerants. Available online: https://www.honeywell-refrigerants.com/europe/product/tag/all-refrigerants/ (accessed on 16 April 2018).
30. 33 Lemmon, E.W.; Huber, M.L.; McLinden, M.O. *Reference Fluid Thermodynamic and Transport Properties, Nist Standard Reference Database 23, Version 9.1*; Physical and Chemical Properties Division, NIST: Boulder, CO, USA, 2002.
31. Chen, J.; Havtun, H.; Palm, B. Investigation of ejectors in refrigeration system: Optimum performance evaluation and ejector area ratios perspectives. *Appl. Therm. Eng.* **2014**, *64*, 182–191. [CrossRef]
32. Shestopalov, K.O.; Huang, B.J.; Petrenko, V.O.; Volovyk, O.S. Investigation of an experimental ejector refrigeration machine operating with refrigerant R245fa at design and off-design working conditions. Part 2. Theoretical and experimental results. *Int. J. Refrig.* **2015**, *55*, 212–223. [CrossRef]
33. Varga, S.; Lebre, P.S.; Oliveira, A.C. Readdressing working fluid selection with a view to designing a variable geometry ejector. *Int. J. Low Carbon Technol.* **2013**, *10*, 205–215. [CrossRef]
34. Huang, B.J.; Ton, W.Z.; Wu, C.C.; Ko, H.W.; Chang, H.S.; Hsu, H.Y.; Liu, J.H.; Wu, J.H.; Yen, R.H. Performance test of solar-assisted ejector cooling system. *Int. J. Refrig.* **2014**, *39*, 172–185. [CrossRef]
35. Huang, B.J.; Wu, J.H.; Hsu, H.Y.; Wang, J.H. Development of hybrid solar-assisted cooling/heating system. *Energy Convers. Manag.* **2010**, *51*, 1643–1650. [CrossRef]
36. Martin, H. A theoretical approach to predict the performance of chevron-type plate heat exchangers. *Chem. Eng. Process. Process Intensif.* **1996**, *35*, 301–310. [CrossRef]
37. Park, J.H.; Kim, Y.S. Evaporation heat transfer and pressure drop characteristics of R-134a in the oblong shell and plate heat exchanger. *KSME Int. J.* **2004**, *18*, 2284–2293. [CrossRef]
38. Kakaç, S.; Liu, H.; Pramuanjaroenkij, A. *Heat Exchangers: Selection, Rating, and Thermal Design*; CRC Press: Boca Raton, FL, USA, 2002.
39. Cooper, M.G. Saturation nucleate pool boiling-a simple correlation. *IChemE Symp. Ser.* **1984**, *86*, 786.
40. Dittus, F.W.; Boelter, L.M.K. Heat transfer in automobile radiators of the tubular type. *Int. Commun. Heat Mass Transf.* **1985**, *12*, 3–22. [CrossRef]
41. Wang, C.C.; Chi, K.Y.; Chang, C.J. Heat transfer and friction characteristics of plain fin-and-tube heat exchangers, part II: Correlation. *Int. J. Heat Mass Transf.* **2000**, *43*, 2693–2700. [CrossRef]

42. Shah, M.M. A general correlation for heat transfer during film condensation inside pipes. *Int. J. Heat Mass Transf.* **1979**, *22*, 547–556. [CrossRef]
43. Quoilin, S.; Declaye, S.; Tchanche, B.F.; Lemort, V. Thermo-economic optimization of waste heat recovery Organic Rankine Cycles. *Appl. Therm. Eng.* **2011**, *31*, 2885–2893. [CrossRef]
44. Botticella, F.; De Rossi, F.; Mauro, A.W.; Vanoli, G.P.; Viscito, L. Multi-criteria (thermodynamic, economic and environmental) analysis of possible design options for residential heating split systems working with low GWP refrigerants. *Int. J. Refrig.* **2018**, *87*, 131–153. [CrossRef]
45. Wildi-Tremblay, P.; Gosselin, L. Minimizing shell-and-tube heat exchanger cost with genetic algorithms and considering maintenance. *Int. J. Energy Res.* **2007**, *31*, 867–885. [CrossRef]
46. Besseghini, S.; Castelli, G.; Guerrini, A.; Poletti, C.; Saglia, S. *Autorità di Regolazione per Energia Reti e Ambiente. Relazione Annuale*; Stato dei servizi; ARERA: Milan, Italy, 2019; Volume 1, Available online: https://www.arera.it/allegati/relaz_ann/19/RA19_volume1.pdf (accessed on 22 January 2020).